D3.1 Simulation model of typical indoor scenario

Thomas Eibert, Han Na, Matthias Saurer, Quanfeng Wang

Grant Agreement Number	101099491
Action Acronym	HOLDEN
Action Title	Ethical Design of Holography with Dense wireless Networks (HOLDEN)
Funding Scheme	HORIZON-EIC-2022-PATHFINDEROPEN-01
Version date of the Annex I against which the assessment will be made	13/12/2022
Start date of the project	1/6/2023
Due date of the deliverable	31/01/2024
Actual date of submission	5/02/2024
Responsible	TUM
Contributors	TUM
Dissemination level	Public

European Innovation Council

Funded by the European Union

Funded by the European Union. Views and opinions expressed are, however, those of the author(s) only and do not necessarily reflect those of the European Union or European Innovation Council and SMEs Executive Agency (EISMEA). Neither the European Union nor the granting authority can be held responsible for them. Grant Agreement No: 101099491.

Authors in alphabetical order

Full Name	Organisation	E-mail
Thomas Eibert	TUM	eibert@tum.de
Han Na	TUM	han.na@tum.de
Matthias Saurer	TUM	matthias.saurer@tum.de
Quanfeng Wang	TUM	quanfeng.wang@tum.de

Change History

Version	Date	Status	Author (Company)	Description
1.0	21.01.2024	Final	TUM	First final version

Executive Summary

Utilizing radio frequency (RF) signals, as, e.g., those from Wi-Fi, in indoor scenarios for tasks like localization or presence/gesture detection has gained much attention in recent years. For the systematic investigation and for thorough understanding of the related methodologies, it is mandatory to have powerful techniques for the accurate simulation of RF signal propagation in the relevant application scenarios, which are typically very complex. Due to the large electrical sizes of these scenarios, full-wave simulations, such as those based on the method of moments (MoM) or finite element methods (FEM), are particularly demanding and, thus, not very desirable for the rapid prototyping of imaging algorithms or of methodologies for the analysis of the propagation channel dynamics. This document presents an efficient simulation framework by the virtue of a ray tracing engine, which allows for an efficient simulation of complex indoor scenarios. The proposed framework seamlessly integrates geometrical optics (GO) and physical optics (PO) by strategically applying the Huygens principle, achieving a well-balanced compromise between efficiency and accuracy. Notably, the implementation leverages a highly parallelized general-purpose ray tracing engine, OptiX™ by NVDIA, resulting in excellent performance. This guarantees quick and reliable data generation, which is especially beneficial for quick prototyping and developing new imaging methods. This is of great relevance for the success of the HOLDEN project.

The following contents are covered:

- Short introduction of the HOLDEN project and the collaboration partners
- A theoretical background of the proposed simulation framework
- Several simulations of electrically small and electrically large objects
- Validation of the simulation methods by reconstructing holographic images

Table of Contents

Abbreviations

Abbreviation	Description
3D	three-dimensional
Aalto	Aalto University
BPA	back projection algorithm
CNR	Consiglio Nazionale Ricerche
EC	European Commission
EM	electromagnetic
EU	European Union
FEM	finite element method
FIAFTA	fast irregular antenna field transformation algorithm
GO	geometrical optics
GTD	geometrical theory of diffraction
HE	Horizon Europe
HOLDEN	Ethical design of holography in dense wireless networks
MIMO	multiple input multiple output
MLFMM	multilevel fast multipole method
MoM	method of moments
PEC	perfect electric conductor
RF	radio frequency
SBR	shooting and bouncing rays
TUM	Technical University of Munich
TWE	University of Twente

UTD	uniform geometrical theory of diffraction
WP	work package

1. Introduction

1.1. About HOLDEN

The ubiquitous perception by sensing of objects, subjects and gestures is a pivotal challenge for future technology: it enables personalized services such as smart living, automated logistics or interaction through free-space gestures. However, it also challenges ethical and moral boundaries and threatens privacy. HOLDEN proposes a radically new approach to perception by concisely analysing ethical constraints and privacy risks while re-thinking RF-based sensing. We establish necessary conditions for privacy preserving and ethically compliant sensing and develop new paradigms respecting these constraints.

For the first time ever, HOLDEN constitutes a concentrated effort to explore social aspects of RF-sensing to guide the technological advance and to derive technology for ethically and privacy compliant perception. Central to HOLDEN is the development of ethical and privacy constraints. We use these findings to derive privacy and ethically compliant concepts for RF-based perception. We will develop a system of distributed multi-antenna devices for simultaneous multitarget recognition and ubiquitous perception with unprecedented accuracy, which constitutes a radical paradigm shift from a technology-centric perspective to a privacy-centric one via privacy by design.

HOLDEN achieves this goal along three high risk, complementary, and privacy-centric paths:

Path 1: Continuous-space measurement points: Radio-based 3D vision by holographic image processing of RF wavefronts.

Path 2: Discrete-space measurement points: Advanced 3D beamforming for human-scale recognition and tracking through dense massive connected antenna arrays.

Path 3: Signal processing and learning: High-dimensional tensor processing for the distinction of complex activities and motion from massive-dimensional RF data. The resulting breakthrough approaches and algorithms will be compared against application-level benchmarks via usage scenarios in the fields of logistics, smart living, and free-space

1.2. Partners

The consortium consists of four academic partners and a high-tech SME partner: (a) Aalto University (AALTO), Finland, (b) Technical University of Munich (TUM), Germany, (c) Consiglio Nazionale Ricerche (CNR), Italy, (d) University of Twente (TWE), Netherlands, and (e) Adant (Adant), Italy. This consortium features the specialized and complementary expertise required to achieve the project objectives. AALTO will be responsible for the project management (WP1), covered by an experienced and dedicated project manager. Ethical aspects (WP2), will be addressed by TWE (Prof. Ciano Aydin) who is a pioneer in the field. In particular, eventual gender differences in the ethical perception will be taken into account. TUM pioneered RF holography, which makes TUM (Prof. Thomas Eibert) the ideal leader of WP3. In advanced distributed signal and information processing, CNR has through Prof. Stefano Savazzi and Vittorio Rampa more than 14 years of

experience. CNR will lead WP4. Since more than 10 years, AALTO is active in radio sensing and machine learning based activity recognition. This expertise makes AALTO (Prof. Sigg) the ideal leader of WP5. Adant (Daniele Piazza) will contribute to the market analysis, application possibilities, and validation (WP6). Led by AALTO, dissemination with the website as one the media will be addressed by all partners. All academic partners are committed to early publication of results, e.g., via arXiv (open science).

2. Simulation Model of Typical Indoor Scenario

In typical indoor imaging scenarios, such as offices, classrooms, or meeting rooms, the sources of illumination are provided by one or more Wi-Fi routers or other types of RF radiation. Receiving antennas, whether positioned inside or outside the room, collect directly received field contributions together with scattered fields, where especially the scattered fields carry a lot of information about the imaging scenario. The antennas can either be multiple units positioned at various spatial sample points, aligning with imaging needs, or mounted on a movable device that scans different desired positions. The measurements obtained from these antennas are subsequently employed within imaging algorithms to reconstruct a holographic 3D image of the objects within the room, or the dynamics of the signals may be analyzed in order to retrieve information about the scenario. Given the long time required for real measurements, virtual measurements by means of powerful simulation techniques appear to be a promising alternative towards the collection of relevant test data. Moreover, the simulations have the advantage that very specific effects can be studied systematically without measurement errors and parasitics. As such, the generation of synthetic measurement data by powerful simulations facilitates rapid prototyping and algorithm test for holographic imaging algorithm development as well as for algorithms analyzing the dynamics of the observation signals [1]. Due to the substantial size of objects relative to the working radiation wavelength, ray-based approaches are effective thanks to the highly localized interaction behaviour of electromagnetic (EM) waves in the high-frequency regime [2]. Therefore, we realize and demonstrate a ray tracing framework for the simulation of EM wave propagation in such indoor scenarios to synthesize virtual measurements. Recognizing the relevance of privacy concerns, our ray tracing framework possesses the capability to simulate through-the-wall wave propagation, thereby enabling virtual measurements for through-the-wall imaging tests as well.

At the core of our implementation lies the Nvidia® CUDA-based, general-purpose ray tracing engine, OptiX™ [3]. The inherent flexibility of OptiX allows for the customization of ray behaviours associated with EM radiation, encompassing physics-based effects such as attenuation, phase shift in free space, and reflection, refraction, and diffraction when interacting with objects of specified material properties. Additionally, the framework supports not only the modelling of realistic objects, but also the definition of virtual surfaces, such as Huygens surfaces and reciprocity surfaces. These surfaces play a pivotal role in collecting and processing EM fields enabling the application of electromagnetic theorems for enhanced field evaluation. Prioritizing ease of use, our code base is designed for accessibility, even for users unfamiliar with OptiX or ray tracing. Users can effortlessly specify geometry, source, and receiver information through a high-level interface. Specifically, one can use our framework either with Julia language [4], application programming interface (API), or configure input parameters via JSON files.

In the upcoming sections, the mathematical foundations of ray tracing simulations will be first reviewed, incorporating the Huygens principle to account for scattering phenomena in a physical optics (PO) sense. Following that, our unique ray tracing strategy will be discussed with rich and straightforward graphical illustrations used to clarify the approach. Subsequently, a series of simulation scenarios will be presented through illustrations of the 3D scene from multiple perspectives, showcasing both ray propagation and the surrounding environment. The reconstructed

image, utilizing EM field information estimated by simulating these virtual measurement setups, will be presented alongside the visualization of the 3D model. This aims to highlight the validity of the ray tracing simulation.

2.1. Theoretical Background

The central objective of our simulation task is to estimate received EM fields with a reasonable level of accuracy in typical indoor imaging scenarios. This enables the testing of imaging algorithms against various scenarios by manipulating the geometry specifications in simulations. This offers a more efficient alternative to physically setting up scenarios and conducting measurements. However, the simulation itself can be time-consuming, necessitating a delicate balance between accuracy and computational complexity.

While the highest accuracy is achieved through full-wave techniques such as the method of moments (MoM) [5], the finite element method (FEM) [6], or finite difference time domain (FDTD) techniques [7], their intrinsic computational complexity poses significant challenges. This complexity becomes particularly pronounced when addressing electrically large problems, as is the case of indoor imaging scenarios, where object dimensions can extend to thousands or more wavelengths. In contrast, approaches utilizing high-frequency approximations, such as geometrical optics (GO) [8] and physical optics (PO) [9], offer enhanced computational efficiency. Although these methods have inherent accuracy limitations, the large and smooth nature of objects in indoor imaging scenarios coupled with appropriate algorithms, allows for reasonably accurate EM results.

Therefore, our emphasis lies on ray-based approaches complemented by PO. The upcoming sections will delve into the theoretical foundations of ray tracing and PO, followed by a detailed exposition of our ray tracing strategy.

2.1.1. Ray Tracing Basics

The ray concept comes from the asymptotic solution to the wave equation in the high-frequency limit [10]. In scenarios where the sizes of the scattering objects are on the order of hundreds or thousands of wavelengths, wave propagation can be effectively modelled as rays—rectilinear propagation paths. Ray tracing, in this context, means identifying such paths that connect radiation source(s) to the targets of interest. Modern ray tracing algorithms, predominantly employing the shooting and bouncing rays (SBR) method [11], initiate numerous rays in random directions from either the transmitter or the receiver side (or both sides [12]). These rays are then tracked, considering line-object intersections, and applying GO rules at each intersection. Upon intersection with an object, each ray bounces by initiating subsequent propagation directions according to GO laws (e.g., the law of reflection, Snell's law, etc.). This process continues until the rays either extend beyond the simulation scope or intersect with meaningful targets, establishing viable paths between the transmitter and the intended targets.

Building upon the identified ray paths, the electric field amplitude along a ray in free space can be derived by observing Fig. 1. As illustrated in the figure, the ray tube cross section increases, where the energy flux through each cross-section surface element is the same. In particular, the energy

flux through the surface element $\mathrm{d}A_0$ is the same as that through the surface element $\mathrm{d}A$, which is given by

$$S\,\mathrm{d}A = S_0\,\mathrm{d}A_0.$$

In the high-frequency limit, the wavefronts are considered as smooth manifolds. Therefore, the surface element can locally be characterized by the principal radii of curvature ρ_1 and ρ_2. Due to the energy conservation, the energy flux density is inversely proportional to the area of the surface element, i.e.,

$$\frac{\|\boldsymbol{S}\|}{\|\boldsymbol{S}_0\|} = \frac{\rho_1\rho_2}{(\rho_1+s)(\rho_2+s)},$$

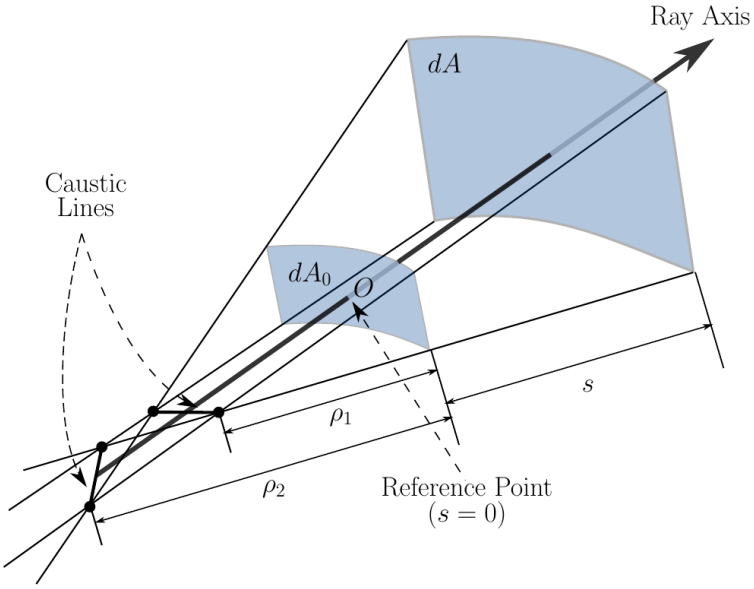

Fig. 1: Astigmatic ray tube valid for a ray along its axis.

where S is the local energy flux density, i.e., the magnitude of the Poynting vector. By Luneberg and Kline [2], the phase evolves proportional to the distance s travelled by the ray. Thus, putting everything together, the complex electric field variation along a ray propagating in free space can be expressed as [2]

$$\boldsymbol{E}(\mathrm{s}) = \boldsymbol{E}_0(0)\sqrt{\frac{\rho_1\rho_2}{(\rho_1+s)(\rho_2+s)}}\,\mathrm{e}^{-\mathrm{j}ks},$$

with $E_0(0)$ being the reference complex electric field amplitude of the ray and s is the parameterization of the length along the ray axis with respect to the reference s=0.

Upon interaction with an object, a ray may undergo reflection, refraction, or diffraction, leading to propagation in new directions in accordance with the Fermat principle. This change in propagation is accompanied by an update to the reference complex electric field amplitude, leveraging the localized behaviour of EM waves in the high-frequency limit. In particular, the pure ray-based approaches consider diffraction via the geometrical theory of diffraction (GTD) [13] or the uniform geometrical theory of diffraction (UTD) [14], where multiple diffracted rays are initiated from the ray-wedge intersection point, as illustrated in Fig. 2.

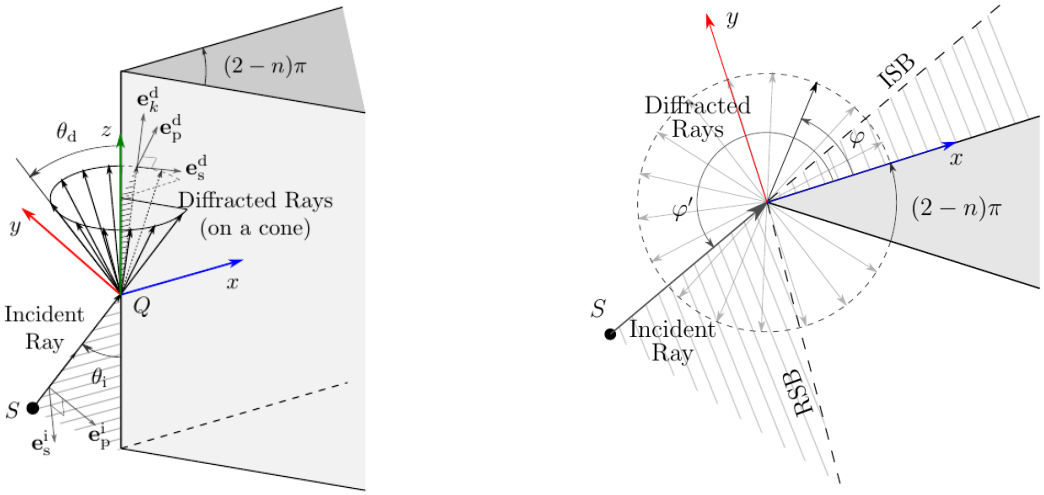

Fig. 2. Illustration of ray-based modelling of wedge diffraction.

2.1.2. Physical Optics

Physical optics (PO) also stems from the high-frequency approximation of wave solutions, where the scattered fields from a surface S are estimated via the integral [9]

$$\boldsymbol{E}^{\mathrm{s}}(\boldsymbol{r}) = \frac{\mathrm{j}k}{2\pi}\iint_S \frac{\mathrm{e}^{-\mathrm{j}kr}}{r}\hat{\boldsymbol{r}} \times (-\hat{\boldsymbol{n}} \times \boldsymbol{E}_{\mathrm{i}}(\boldsymbol{r}'))\,\mathrm{d}S,$$

where $\boldsymbol{r}$ and $\boldsymbol{r}'$ denote the positions of the observation point and the equivalent source, respectively, and r is the distance between $\boldsymbol{r}$ and $\boldsymbol{r}'$. The unit vectors $\hat{\boldsymbol{r}}$ and $\hat{\boldsymbol{n}}$ correspond to the direction from the source to the observation point and the surface normal at $\boldsymbol{r}'$, respectively. The physical interpretation of the integral involves the superposition of radiation from all equivalent surface currents, which are given by [2]

$$\boldsymbol{M}_S(\boldsymbol{r}') = -\hat{\boldsymbol{n}} \times \boldsymbol{E}_{\mathrm{i}}(\boldsymbol{r}').$$

This relationship models the wave behaviour better because the incident wave, even originally in a single direction, triggers scattered waves in all directions, in contrast to the mirror-like behaviour of pure ray-based approaches, where the scattered wave is only found along a single direction which makes the same angle with the normal as the incident ray. However, PO, in its conventional form, assumes that surface currents are only induced by the incident wave, implicitly ignoring secondary effects from other induced surface currents. In other words, multipath effects are ignored. This limitation is conventionally addressed by iterative PO, which considers secondary effects by iteratively updating surface currents [9]. However, this approach can be computationally expensive and may not always converge, hence, limiting its practicality.

To overcome this limitation, we turn to a more fundamental principle, namely the Huygens principle also known as equivalence principle [15]. This principle states that every point reached by a luminous disturbance becomes a new source of an elementary wave. Mathematically, this can be expressed as an integral over a closed surface S [2]

$$\boldsymbol{E}(\boldsymbol{r}) = \iint_S [\overline{\boldsymbol{G}}_J^E(\boldsymbol{r},\boldsymbol{r}') \cdot \boldsymbol{J}_S(\boldsymbol{r}') + \overline{\boldsymbol{G}}_M^E(\boldsymbol{r},\boldsymbol{r}') \cdot \boldsymbol{M}_S(\boldsymbol{r}')]\mathrm{d}s',$$

where $\overline{\boldsymbol{G}}_J^E$ and $\overline{\boldsymbol{G}}_M^E$ are the dyadic Green's functions of the electric field due to electric and magnetic surface current densities, $\boldsymbol{J}_S$ and $\boldsymbol{M}_S$, respectively. One can derive the PO integral using the Huygens principle by choosing the Huygens surface S tightly wrapping the surface of the scattering object and let $\overline{\boldsymbol{G}}_J^E$ and $\overline{\boldsymbol{G}}_M^E$ take the form of the free-space Green's function.

Since the Huygens principle is universal, S can be an arbitrary closed surface, which does not have to tightly wrap the scattering object. This flexibility allows us to select a surface enclosing a wide region containing multiple scattering objects, while leaving observation points outside. For example, one could even choose a plane that extends to infinity. As illustrated in Fig. 3 (a)-(d), the transmitter and the receiver are in the left half space, and the scattering object of interest is in the right half space.

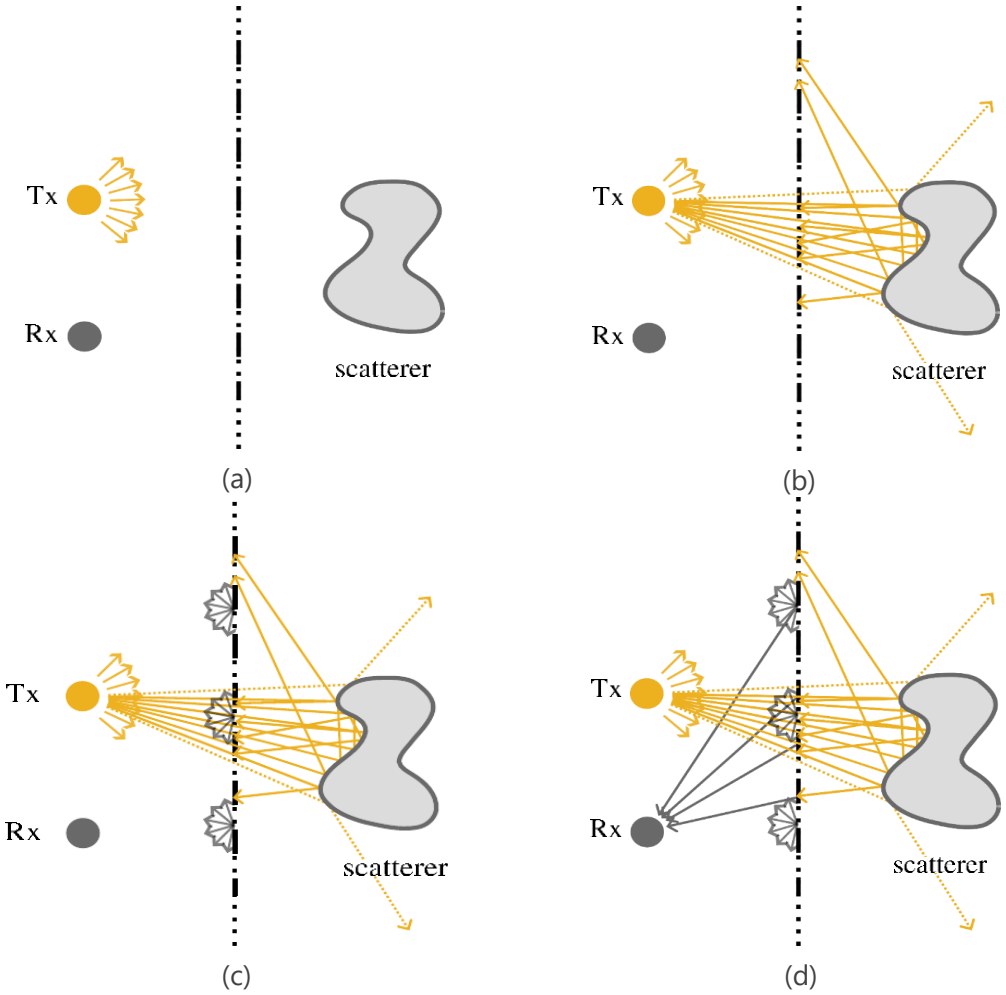

Fig. 3. Ray-PO hybrid approach using the Huygens principle: (a) rays initiated from the source, (b) rays interact with objects of interest, and bounce back, (c) equivalent sources initiated on the Huygens surface, (d) evaluate the final received field by adding up field contributions from all equivalent sources.

With this setup, the incident fields can be modelled as rays entering the domain enclosed by the Huygens surface. The interaction between the incident wave and scattering objects can then be handled in a ray-based approach, as discussed in the previous section. Rays bouncing off the object

and intersecting the Huygens surface from inside are collected, and their associated EM fields are employed in a Huygens' integration over the surface, providing an estimation of the final received fields.

This hybrid approach has advantages of both traditional shooting and bouncing ray tracing and physical optics: on the one hand, the rays bouncing within the region enclosed by the Huygens surface take multipath effects into account. On the other hand, performing the Huygens' integration over the surface considers the wave scattering effects in a physical optics sense, enhancing the accuracy of the pure ray-based approaches.

2.2. Ray Tracing Framework

As depicted in Fig. 4, the general workflow of our ray tracing framework unfolds in three fundamental steps. In the initial stage, the setup of the geometry, the positions of transmitters (Tx) and receivers (Rx) are entailed into the simulation. Following this, rays are launched from the transmitters in random directions, traversing through the Huygens surface that encapsulates the scattering objects. These rays interact with the surfaces of the scattering objects, undergoing reflections, refractions, and/or diffractions in geometric optics sense. Rays that bounce off the objects and intersect the Huygens surface from the inside are collected. Subsequently, equivalent surface currents are initiated at the Huygens surface, encoding the scattering phenomena taking place at the objects. In the final stage, rays are launched from these equivalent surface current sources, directed toward the receivers, where the received fields from all Huygens sources are accumulated coherently.

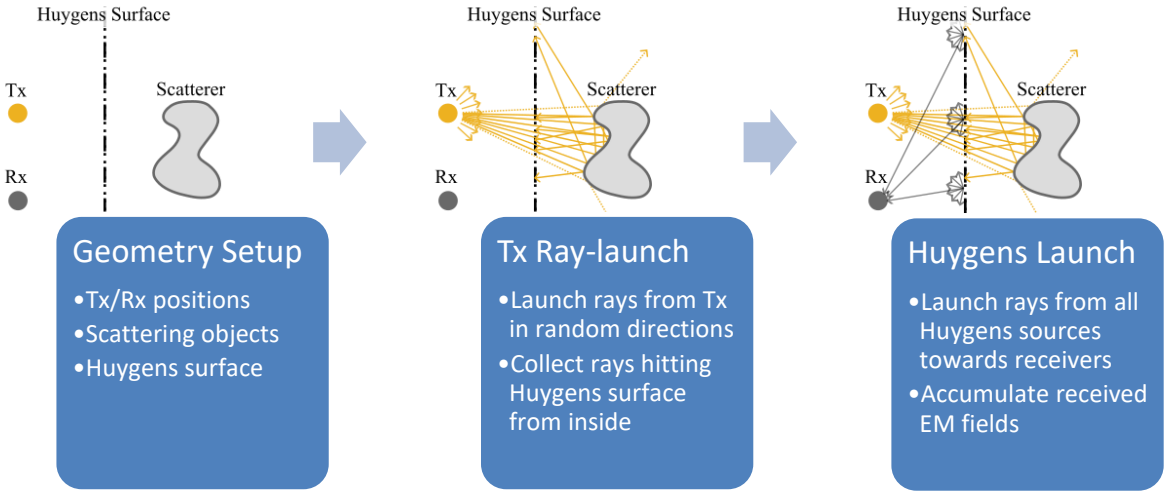

Fig. 4. Workflow of the proposed ray tracing framework.

Functionality-wise, these steps are implemented in two primary components: 1. path tracing for geometric optics considerations; 2. EM calculation based on the Huygens principle in a physical

optics sense. The first component relies on the Nvidia CUDA-based, general-purpose ray tracing engine, OptiX. This engine computes ray propagation paths, efficiently solving numerous straight-line-mesh intersections in parallel. Benefitting from the hardware and software optimization of OptiX, this part achieves very high efficiency. Additionally, the general-purpose nature of OptiX allows us to define various ray behaviours, including phase evolution, attenuation, and on-the-fly evaluations of reflection, refraction, and diffraction coefficients. The second component, the EM calculation, which has already mentioned is based on Huygens principle, is partially integrated with OptiX. It involves the on-the-fly accumulation of field contributions from different equivalent Huygens sources.

On top of this kernel, we have also implemented a Julia interface that manages the simulation setups, covering aspects like geometry, source, and receiver specifications. Users enjoy considerable freedom in defining the Huygens surface through the intuitive Julia interface. This streamlined approach facilitates tasks such as pre-processing geometry data, selecting simulation parameters, and post-processing results. The framework adheres to a typical "application programming interface" (API) structure, empowering users to create customized simulation scripts. This structure facilitates iteration over various setups, allowing, for example, looping over different scenarios. The rich package ecosystem of Julia language ensures the seamless import of various geometry data types, encompassing formats like OBJ and STL files. Additionally, users can export final or intermediate results into diverse formats, such as MAT files and npz files. These result files are compatible with various software, including MATLAB™ [16]. Given that we have implemented imaging algorithms in MATLAB, using the simulation results in the imaging routines is straightforward.

The effectiveness of our EM computations transcends imaging scenarios [1]. A robust validation comes from its successful application in urban pathloss prediction, as evidenced by comparisons with actual measurements in Munich city that affirm its accuracy [17]. Notably, the software demonstrates exceptional performance even when handling multiple stacked Huygens surfaces, a necessity for such intricate predictions. This proven accuracy increases confidence and reliability when employed with a single Huygens surface in our imaging scenarios. Furthermore, findings from [18] underscore the precision of Huygens surface integration in ray tracing, particularly in non-shadow regions or optical boundaries—conditions fits in most of our imaging setup.

2.3. Numerical Examples

This section presents numerical examples using three simulation methods: 1. full-wave simulations with FEKO™ [19]. This approach offers good accuracy, but its main limitation is the large computational expense associated with electrically large problems, even with the assistance of multilevel fast multipole method (MLFMM); 2. conventional PO with a naive direct summation implementation, validated for simple geometries, but cannot handle multipath effects; 3. our ray tracing framework, showing a good compromise between balancing accuracy and efficiency. These examples demonstrate our capability to produce well focused images using different approaches, allowing us to generate physically consistent output data for different imaging algorithms. While we recommend our hybrid ray tracing method with Huygens integral especially for the context of large-scale scenarios, we acknowledge the versatility of other methods for specific scenarios. The subsequent subsections delve into specific details of each simulation approach and give also deeper insights into the different imaging methods we used for verification.

2.3.1. Full-wave simulations

In this section, an imaging setup involving three electrically small PEC spheres illuminated by a Hertzian dipole is considered. As illustrated in Fig. 5, a y-polarized Hertzian dipole, represented by a yellow arrow, is positioned at $(-0.5\ \mathrm{m}, 0\ \mathrm{m}, 0.5\ \mathrm{m})$. The three spherical scatterers are centred at $(0\ \mathrm{m}, 0\ \mathrm{m}, 0\ \mathrm{m})$, $(0.3\ \mathrm{m}, 0\ \mathrm{m}, 0\ \mathrm{m})$, and $(0.6\ \mathrm{m}, 0\ \mathrm{m}, 0\ \mathrm{m})$, respectively. The radius of each scattering sphere is $0.01\ \mathrm{m}$. The EM field information is collected over a closed spherical surface with a radius of $0.7\ \mathrm{m}$. The radiation frequency spans from $8\ \mathrm{GHz}$ to $10\ \mathrm{GHz}$. Given the simplicity of the scenario and its relatively small electrical size, a full-wave simulation is feasible. We conducted the full-wave simulation using the commercial software FEKO and utilized the resulting EM fields for imaging.

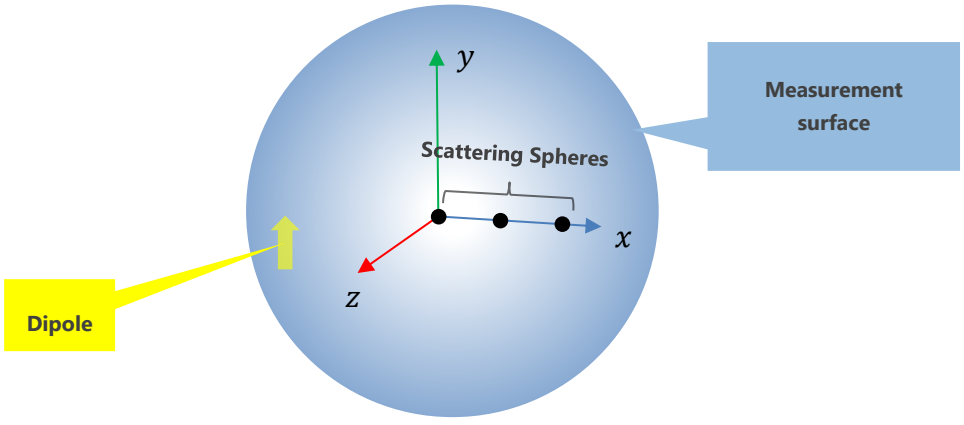

Fig. 5. Simulation configuration in FEKO.

The obtained magnitudes of the scattering field over the measuring surface are shown in Fig. 6.

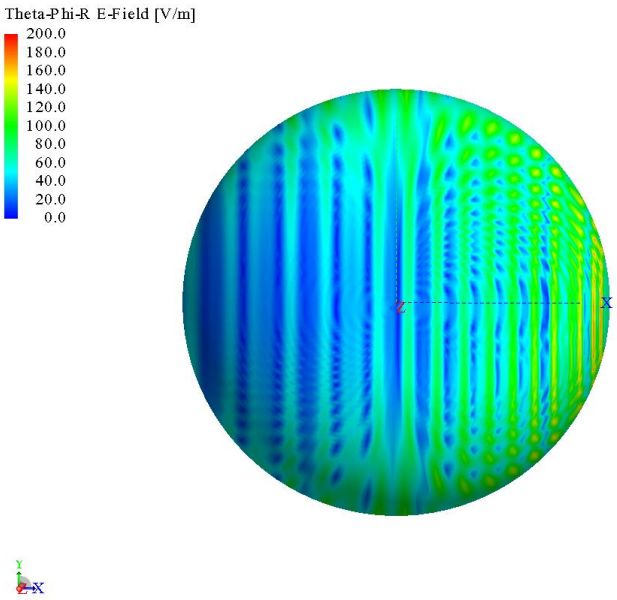

Fig. 6. Simulated scattering field from FEKO.

Selecting a single probe signal, for example, at the position $(0\ \mathrm{m}, 0\ \mathrm{m}, 0.7\ \mathrm{m})$, and applying the inverse Fourier transform results in a time-domain signal, which is shown in Fig. 7.

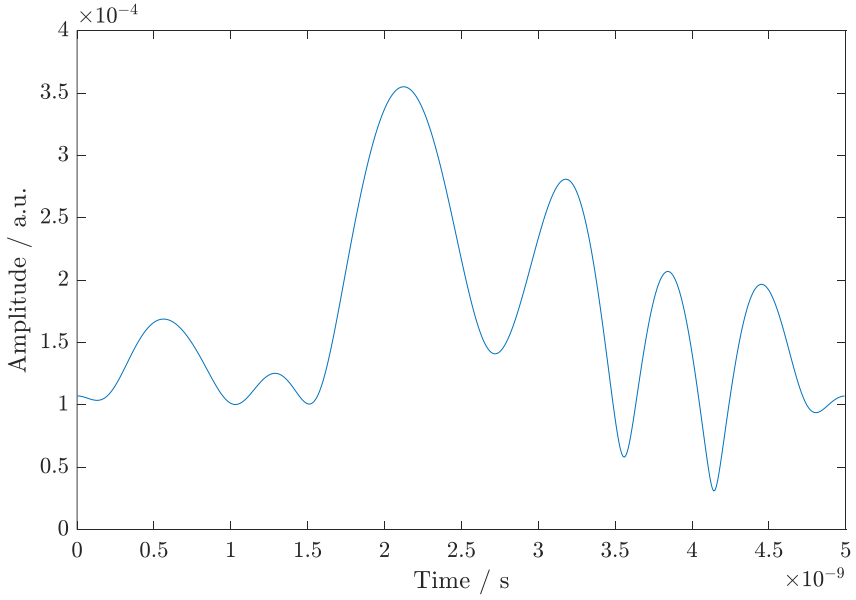

Fig. 7. Signal at the position $(0\ \mathrm{m}, 0\ \mathrm{m}, 0.7\ \mathrm{m})$ in time domain.

It is obvious that three peaks, representing these three scatterings, are shown in the figure. Due to the limited time-domain resolution, mutual coupling between scatterers and other factors, a noise peak also appears in Fig. 7.

Despite the geometric simplicity of the scenario, the imaging is challenging due to the dominant direct incident field from the source. Special considerations, such as echo suppression [20], are implemented to retrieve the scattered field with high fidelity using our inverse solver FIAFTA [21]. Imaging results using single-frequency EM data at $10\ \mathrm{GHz}$ is illustrated in Fig. 8, where the positions and sizes of the scatterers are clearly visible.

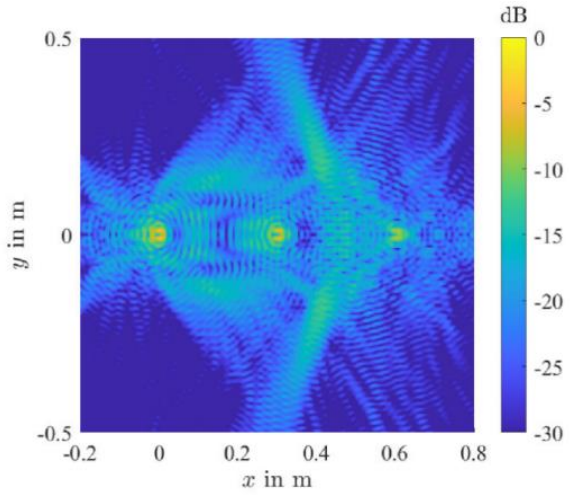

Fig. 8. Spatial image of $\|E\|$ at $10\ \mathrm{GHz}$ along the x- y-plane.

To enhance image quality, multiple-frequency data are synthesized. By applying phase correction for each individual scattering sphere, one can obtain images focusing on different target, as illustrated in Fig. 9 (a)-(c).

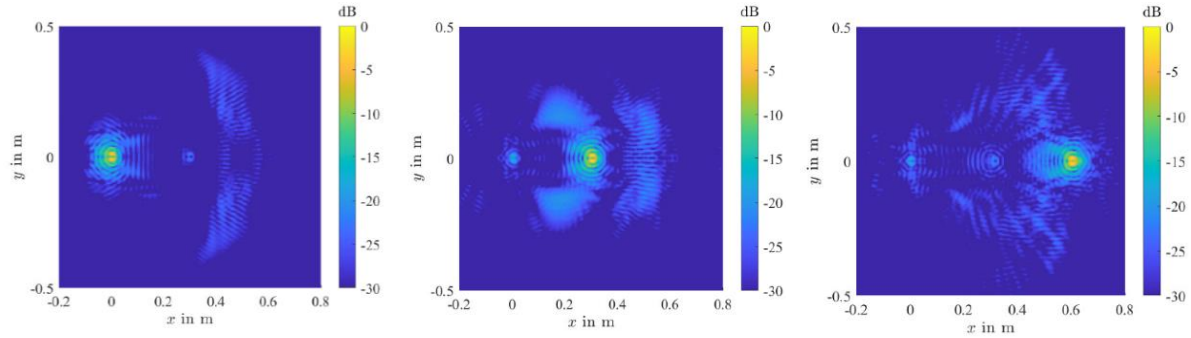

(a) (b) (c)

Fig. 9. Spatial images of the spheres along the xy-plane. The different phase correction factors are applied to achieve different focusing points. The utilized frequencies span from $\mathbf{8}\ \mathrm{GHz}$ to $10\ \mathrm{GHz}$, with a step of $0.2\ \mathrm{GHz}$.

In order to obtain a clear image for all three spheres, phase correction factors must be applied for each pixel, as demonstrated in Fig. 10.

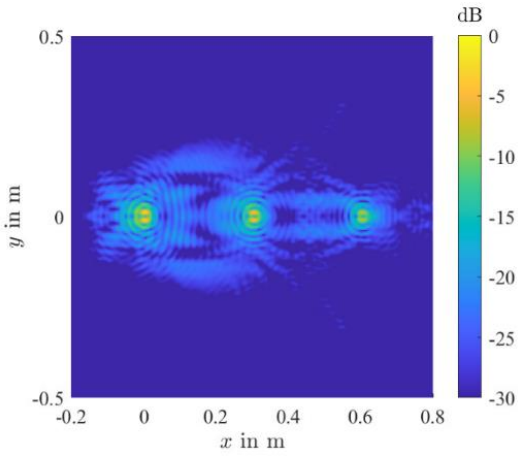

Fig. 10. Multiple frequency image with position dependent phase adjustment.

2.3.2. Physical Optics simulations

This section delves into diverse imaging scenarios, each featuring distinct scatterers for imaging within a consistent transmitter-receiver setup. As illustrated in Fig. 11, our configuration involves 160 transmitters and 160 receivers equidistantly positioned along the red and blue edges of the rectangular imaging aperture. Aligned with the xy-plane at a height of $50\ \mathrm{cm}$, these transmitters and receivers facilitate the transmitting and receiving of EM waves of frequencies ranging from $20\ \mathrm{GHz}$ to $28.3\ \mathrm{GHz}$. A dedicated PO simulation is performed for each scenario, estimating the received E-field for every transmitter-receiver pair at each frequency. Subsequently, the resulting data are fed into holographic imaging routines to generate insightful 3D images.

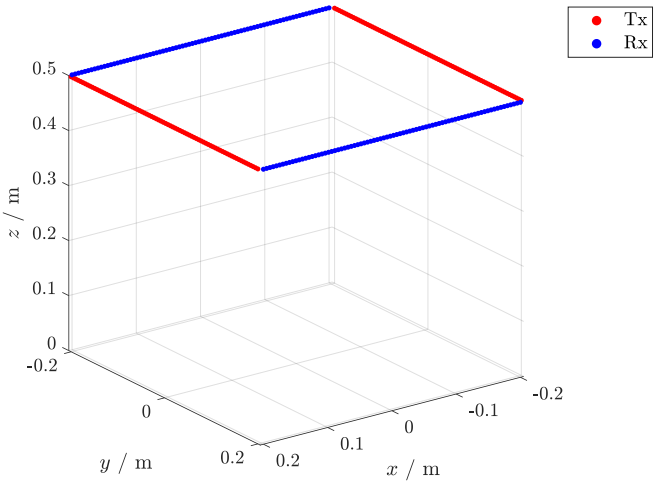

Fig. 11. Transmitter-receiver configuration for the following imaging scenarios.

In the PO evaluation, we employ a naive Monte-Carlo method. This involves the summation of numerous random samples of equivalent surface currents, expressed as

$$\boldsymbol{E}^{\mathrm{s}}(\boldsymbol{r}) = \frac{-\mathrm{j}k}{2\pi} \sum_{i=1}^{N} \frac{\mathrm{e}^{-\mathrm{j}k\|\boldsymbol{r}-\boldsymbol{r}_i'\|}}{\|\boldsymbol{r}-\boldsymbol{r}_i'\|} \hat{\boldsymbol{r}}_{\boldsymbol{i}} \times (\hat{\boldsymbol{n}} \times \boldsymbol{E}_{\mathrm{i}}(\boldsymbol{r}_i')) \, \Delta S_i,$$

where $\boldsymbol{E}_{\mathrm{i}}(\boldsymbol{r}_i')$ represents the incident electric field at position $\boldsymbol{r}_i'$ on the scattering surface from a certain transmitter, and ΔS_i denotes the area associated with the i-th sample. The incident field is treated as entirely generated by the transmitter and can be evaluated via

$$\boldsymbol{E}_{\mathrm{i}}(\boldsymbol{r}') = \frac{\mathrm{e}^{-\mathrm{j}k\|\boldsymbol{r}'-\boldsymbol{r}_{\mathrm{tx}}\|}}{\|\boldsymbol{r}'-\boldsymbol{r}_{\mathrm{tx}}\|} \boldsymbol{E}_0(\vartheta, \varphi),$$

where $\boldsymbol{E}_0(\vartheta, \varphi)$ denotes the electric field at a unit distance away from the transmitter in the direction (ϑ, φ) pointing to the point $\boldsymbol{r}'$ on the scattering surface.

In the following examples, two different imaging algorithms are used to perform the image creation. One is the back-projection algorithm (BPA) [22], which directly transforms the simulation data in an image in spatial domain. The other method which we wanted to consider is the multi-input-multi-output ω- k-algorithm (MIMO-ω- k) [23], which works based on a plane-wave expansion of the transmitting and receiving array.

Example 1. Flat star shaped PEC sheet

The imaging configuration is illustrated in Fig. 12, where the target for imaging is a flat star shaped PEC sheet, placed in xy-plane, and centred around the coordinate origin. The reconstructed images for this example are depicted in Fig. 13 (a) and (b). As can be seen, the shape of the star is clearly visible, and the depth extent (z-direction) of the PEC sheet is also well captured.

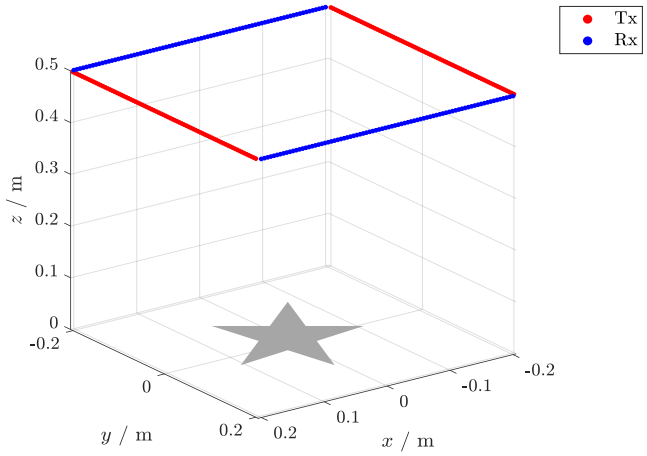

Fig. 12. Imaging setup for a flat star-shaped PEC sheet.

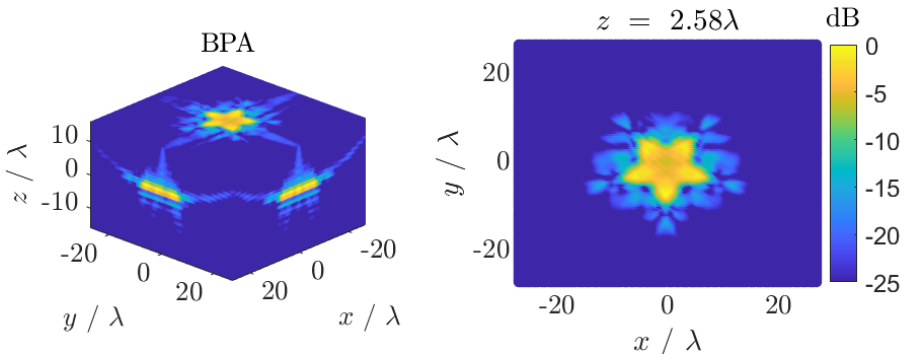

(a) Imaging using BPA.

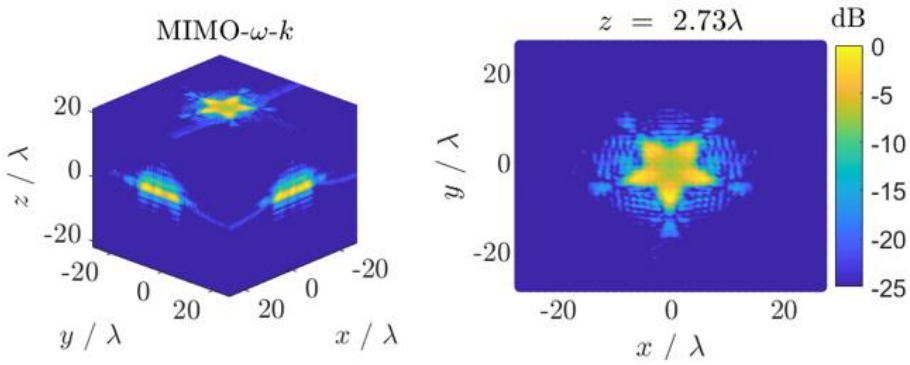

(b) Imaging using MIMO-$\boldsymbol{\omega}$- $\boldsymbol{k}$.

Fig. 13. Imaging for flat star-shaped PEC sheet using BPA and MIMO-ω- k.

Example 2. Spherical PEC cap

The target in this example is a spherical PEC cap with a height of 0.01 m as depicted in Fig. 14. For validation of the PO based ray tracer, the spatial images according to Fig. 15 (a) and (b) were generated. Notably, this example poses greater challenges over the previous one because the shape is not flat, one could clearly see the curvature from the side view of the image, which shows the remarkable fidelity of the simulation.

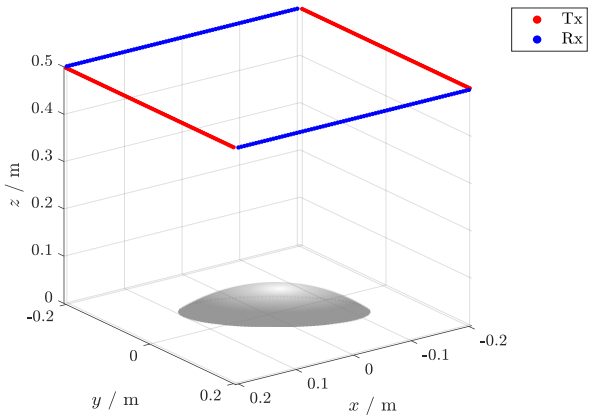

Fig. 14. Imaging setup for a spherical cap with height of 0.01 m.

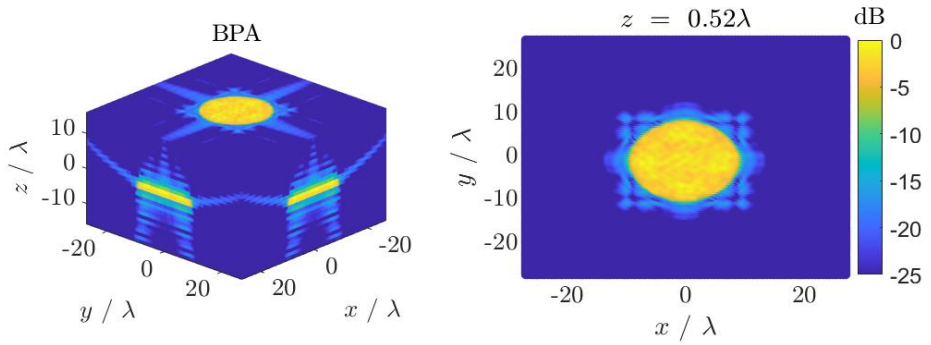

(a) Imaging using BPA.

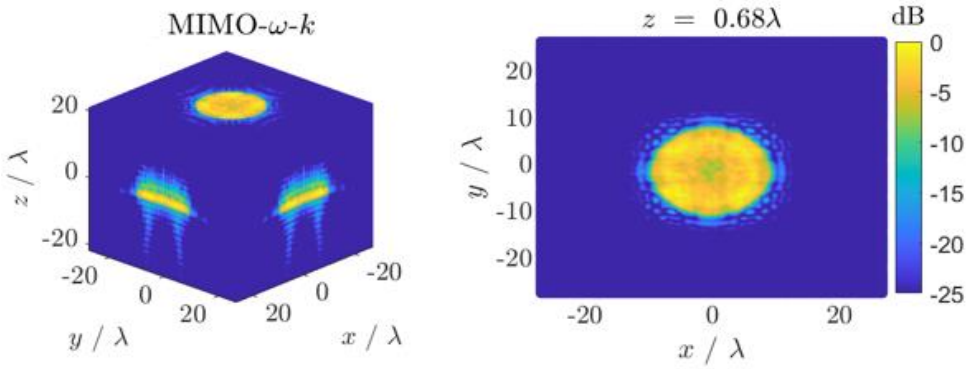

(b) Imaging using MIMO-$\boldsymbol{\omega}$- $\boldsymbol{k}$.

Fig. 15. Imaging for the spherical cap using BPA and MIMO-ω- k.

2.3.3. Simulations by the Hybrid Ray Tracing Framework

For the verification of the hybrid ray tracing framework, this section presents two examples, both featuring a multistatic setup of antenna arrays arranged in a planar configuration. A total of 10 linearly distributed frequency samples ranging from $2401\,\mathrm{MHz}$ to $2423\,\mathrm{MHz}$ are employed, aligning with the first WLAN channel of the IEEE 802.11b standard.

Example 1: Man on a desk next to a sofa

In this simulation, 200 transmitting antennas and 14 112 receiving antennas was configured as is illustrated in Fig. 16(a). The simulation involves launching rays from the antennas towards scattering objects, and the scattered rays, intersecting with the equivalent Huygens surface, are recorded, as depicted in Fig. 16(b). The simulation concludes by evaluating the Huygens integral for all receiver locations, demonstrating the process in Fig. 16 (c).

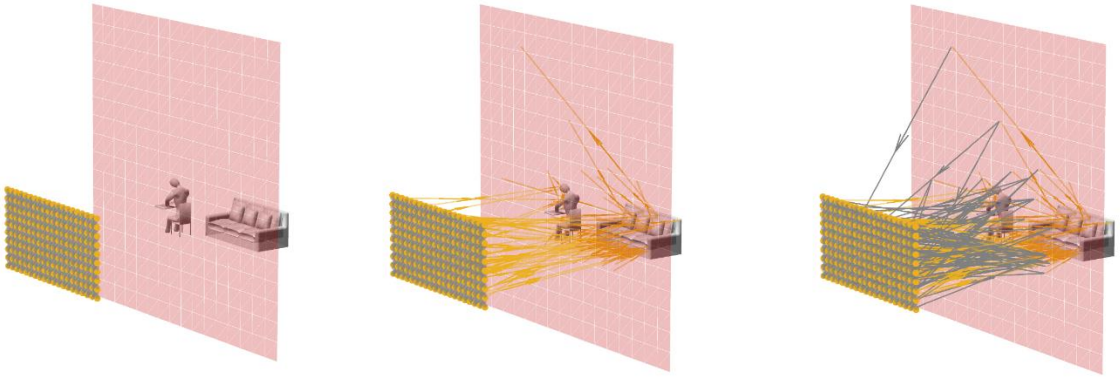

(a) Huygens' surface setup, b) Tx → Scatterer → Huygens, c) Huygens → Rx,

Fig. 16. Ray tracing simulation of a man on a desk next to a sofa.

The resulting E-field at each receiver associated with each transmitter is recorded in an array. An illustrative representation is provided in Fig. 17, where the colormap showcases the magnitude of the backscattered E-field from one of the transmitters.

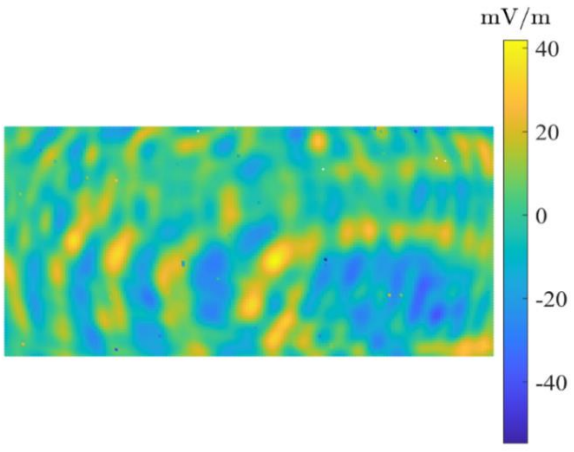

Fig. 17. Back-scattering E-field magnitude of the scene "man on a desk"

To further analyse the simulation, delay spread graphs for each pair of transmitter and receiver were generated by Fourier transforming the E-field signal at different frequency samples. Fig. 18 provides an example, indicating a prominent peak that corresponds to the near-specular reflection of the front face of the sofa or the body. This insightful information enhances our understanding of dominant reflections and their timing within the simulated scenario.

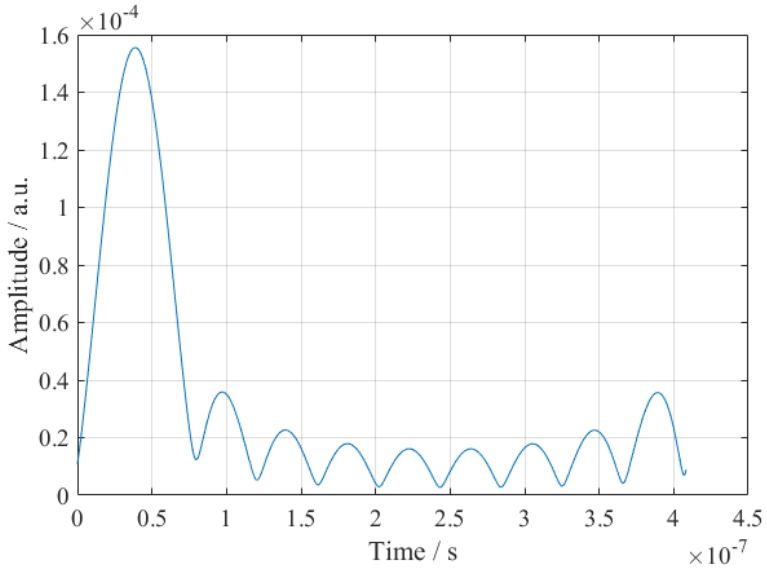

Fig. 18. Time delay spread for one of the Tx-Rx pair in the scene "man on desk"

The microwave images for this case, are generated by an inverse source method [24] as well as the BPA, which are shown in Fig. 19. The images show good focusing and allow for a clear interpretation of the scene and, hence, demonstrating the excellent performance of the utilized ray tracer.

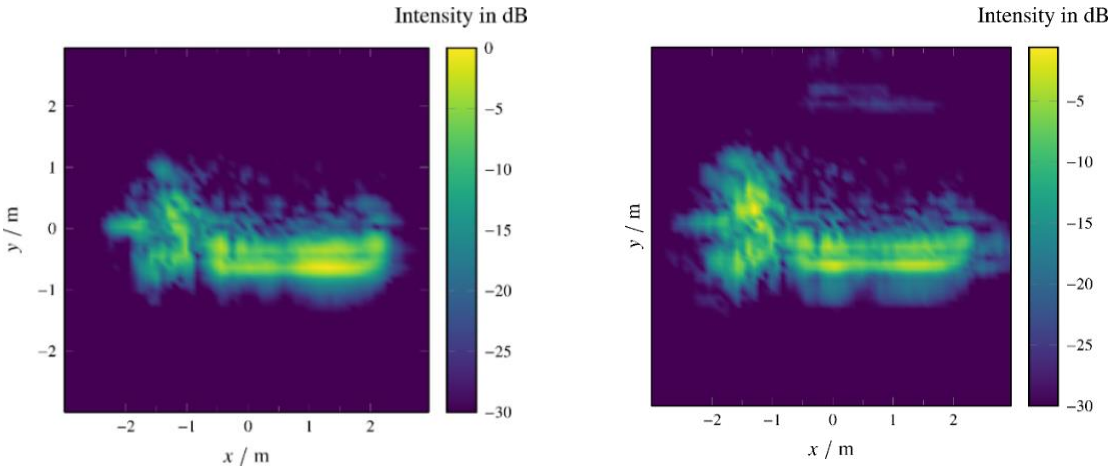

(a) Inverse source solver. (b) BPA.

Fig. 19. Reconstruction results for the scene "man on a desk".

Example 2: Female in free space

The second simulation, which was performed with the hybrid ray tracing engine was a body of a female floating in free space as is depicted in Fig. 20 (a). For this scenario one single transmitter was assumed in the centre of the scene, which was approximately $10\ \mathrm{m}$ away from the target. The forward rays from the source antenna towards the target are drawn in Fig. 20 (b). As in the previous example the scattered rays intersecting with the Huygens surface were collected and recorded for further processing. In Fig. 20 (c) the rays from the Huygens surface to the 262 144 receivers, which are all placed on a regular grid is shown.

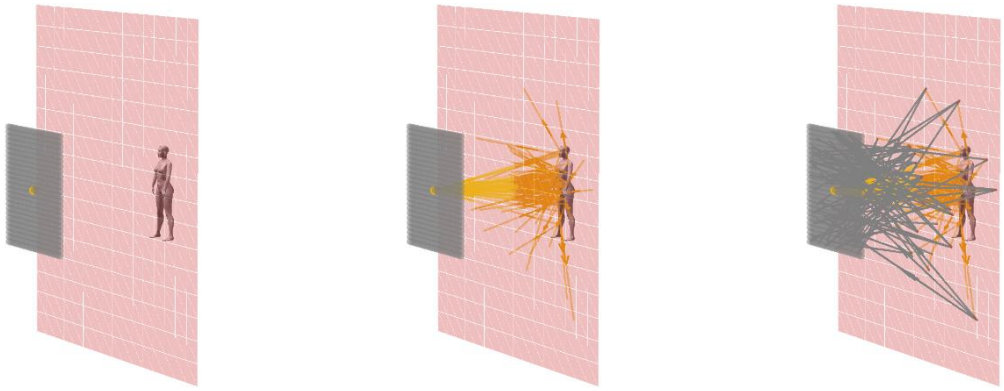

(a) Huygens surface setup. b) Tx → Scatterer → Huygens. c) Huygens → Rx.

Fig. 20. Ray tracing simulation of a woman in free space.

The back-scattering E-field magnitudes at the receivers are illustrated in Fig. 17. For a receiver close to the aperture centre, its received time domain signal strength (or time delay spread) is shown in Fig. 22, where also a dominant peak appears, indicating a strong specular-like reflection from the object.

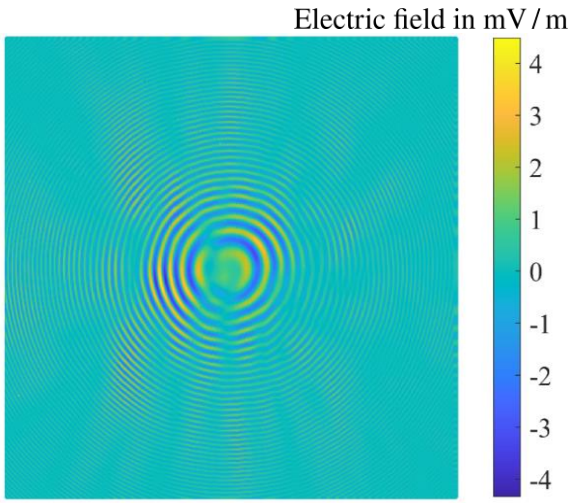

Fig. 21. Back-scattering E-field magnitude of the scene “woman in free space”.

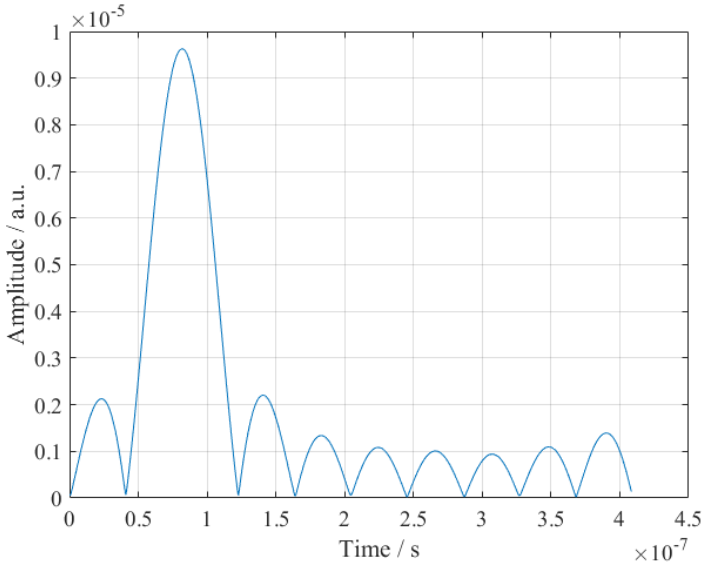

Fig. 22. Time delay spread for one of the Tx-Rx pair in the scene "woman in free space".

As illustrated in Fig. 23, the reconstructed images utilizing again two different reconstruction methods are shown. Interestingly, both spatial images show only good focusing near the chest region of the target, at which most of the forward rays are reflected back to the receiving antennas. By contrast, the rays hitting the extremities like the arms and legs and also the head are mostly reflected away from the antenna array. This is because these body parts show more like a cylindrical shape. However, these observations are inherent to the scattering process itself and do not stem from the ray tracing simulation or the imaging approaches. This example shows the importance of accurately modelling and simulating real-world targets and understanding the scattering mechanism behind it.

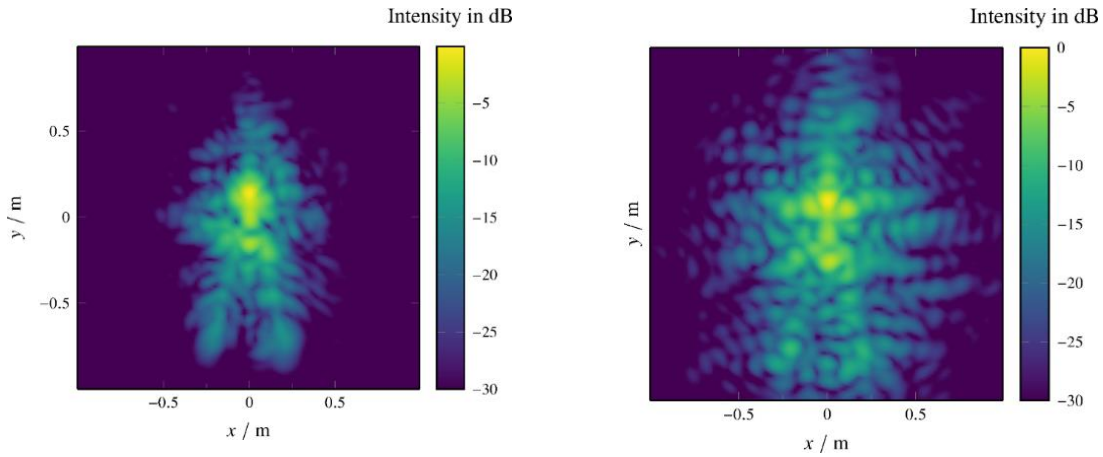

(a) Inverse source solver. (b) BPA.

Fig. 23. Reconstruction results for the scene "woman in free space".

Example 3. Two persons in a classroom

In this scenario, two individuals are situated in a classroom-like setup, modelling the walls, ceiling, floor, desks, and chairs, typical of an indoor environment. As depicted in Fig. 24, a Wi-Fi router inside the room serves as the source (indicated by the red dot), while a set of regularly arranged receivers forms a rectangular aperture, marked by blue dots.

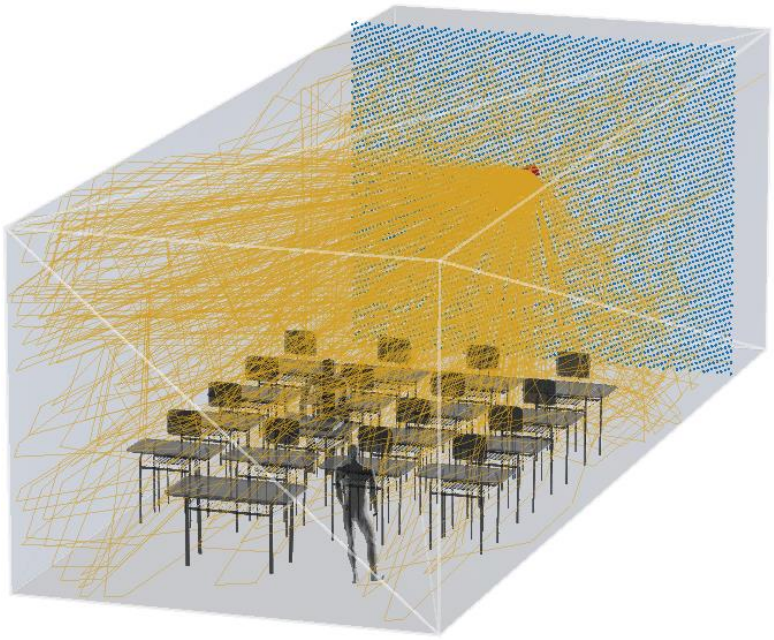

(a) Side view of the classroom scenario.

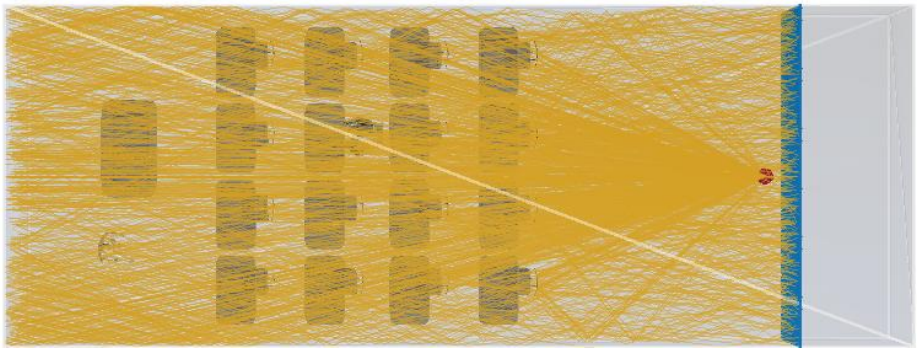

(b) Top view of the classroom scenario.

Fig. 24. Visualization of forward rays from a single illumination source in a complex environment such as a classroom.

The ray paths, illustrated by yellow lines in Fig. 24 , reveal significant multi-path effects caused by reflections between walls, ceilings, and the ground. Rays tend to bounce multiple times, resulting in complicated path patterns.

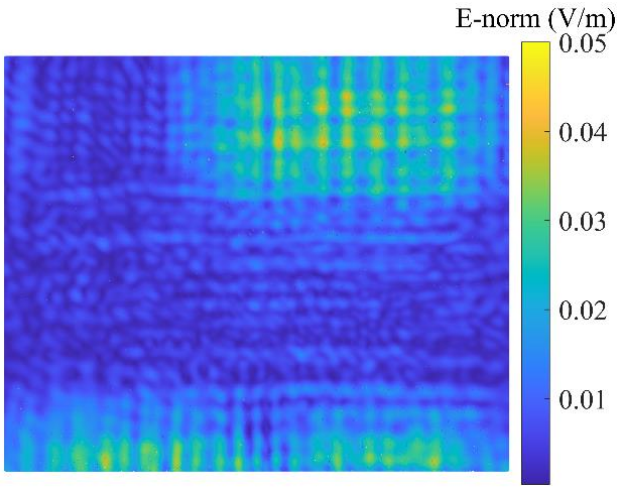

Fig. 25. The received E-field magnitude.

Fig. 25 portrays the magnitude of the backscattered E-field, exhibiting distinctive patterns resembling a grid. These patterns potentially correspond to modes within the rectangular cavity formed by the walls, ceiling, and ground. However, achieving precise imaging using this data poses an ongoing challenge due to the complex interplay of strong multipath effects.

3. Summary

It was demonstrated that various ways of simulating typical indoor propagation scenarios are available, ranging from full-wave simulations to ray tracing approaches. Despite the suitability of alternative methods, our recommended ray-PO hybrid method exhibits a good balance between accuracy and efficiency, as demonstrated by various simulation results. Although our simulations primarily focus on the frequency domain delivering synthetic data as basis for holographic imaging, obtaining the time behaviour is also achievable through Fourier transformation, providing a time delay spread function for dynamic channel analysis.

4. References

[1] H. Na, M. Saurer, and T. F. Eibert, "Electromagnetic ray tracing simulation and imaging of complex indoor scenarios," in *International Conference on Electromagnetics*, pp. 300–302, 2023.

[2] C. A. Balanis, *Advanced Engineering Electromagnetics,* 2nd ed. Hoboken, N.J.: John Wiley & Sons, 2012.

[3] S. G. Parker *et al.*, "OptiX," *ACM Trans. Graph.*, vol. 29, no. 4, pp. 1–13, 2010, doi: 10.1145/1778765.1778803.

[4] J. Bezanson, S. Karpinski, V. B. Shah, and A. Edelman, "Julia: a fast dynamic language for technical computing," 2012.

[5] W. C. Gibson, *The Method of Moments in Electromagnetics*. Boca Raton: CRC Press, 2021.

[6] J.-M. Jin, *Finite element method in electromagnetics,* 3rd ed. Hoboken, N.J.: John Wiley & Sons, 2014.

[7] S. D. Gedney, *Introduction to the Finite-Difference Time-Domain (FDTD) Method for Electromagnetics*. Cham: Springer International Publishing, 2011.

[8] N. Lindlein and G. Leuchs, "Geometrical optics," in *Springer Handbook of Lasers and Optics*, F. Träger, Ed., New York: Springer, 2007, pp. 33–85.

[9] M. Nieto-Vesperinas, *Scattering and Diffraction in Physical Optics*. Madrid: World Scientific, 2006.

[10] A. Sommerfeld and J. Runge, "Anwendung der Vektorrechnung auf die Grundlagen der geometrischen Optik," *Annalen der Physik*, vol. 340, no. 7, pp. 277–298, 1911, doi: 10.1002/andp.19113400705.

[11] H. Ling, R.-C. Chou, and S.-W. Lee, "Shooting and bouncing rays: calculating the RCS of an arbitrarily shaped cavity," *IEEE Trans. Antennas Propag.*, vol. 37, no. 2, pp. 194–205, 1989, doi: 10.1109/8.18706.

[12] M. M. Taygur, I. O. Sukharevsky, and T. F. Eibert, "A bidirectional ray-tracing method for antenna coupling evaluation based on the reciprocity theorem," *IEEE Trans. Antennas Propag.*, vol. 66, no. 12, pp. 6654–6664, 2018, doi: 10.1109/TAP.2018.2876680.

[13] J. B. KELLER, "Geometrical theory of diffraction," *Journal of the Optical Society of America*, vol. 52, pp. 116–130, 1962, doi: 10.1364/JOSA.52.000116.

[14] R. G. Kouyoumjian and P. H. Pathak, "A uniform geometrical theory of diffraction for an edge in a perfectly conducting surface," *Proc. IEEE*, vol. 62, no. 11, pp. 1448–1461, 1974, doi: 10.1109/PROC.1974.9651.

[15] C. Huygens, *Traité de la Lumière*. A Leide: Chez Pierre vander Aa, marchand libraire, 1690.

[16] The MathWorks Inc., *MATLAB*. Natick, Massachusetts, United States: The MathWorks Inc. [Online]. Available: https://www.mathworks.com/

[17] H. Na, M. M. Taygur, and T. F. Eibert, "A multiple Huygens surface based ray tracing framework with GPU acceleration," *IEEE Trans. Antennas Propagat.*, p. 1, 2023, doi: 10.1109/TAP.2023.3326942.

[18] H. Na and T. F. Eibert, "Utilization of multiple Huygens surfaces in ray tracing scenarios involving diffractions," in *Photonics & Electromagnetics Research 2023*, pp. 288–296.

[19] U. Jakobus, A. Aguilar, E. Attardo, M. Schoeman, J. van Tonder, and K. Longtin, "Review of selected new features in FEKO 2018," in *International Applied Computational Electromagnetics*, 2018, pp. 1–2.

[20] J. Knapp and T. F. Eibert, "Near-field antenna pattern measurements in highly reflective environments," *IEEE Trans. Antennas Propagat.*, vol. 67, no. 9, pp. 6159–6169, 2019, doi: 10.1109/TAP.2019.2922548.

[21] T. F. Eibert and C. H. Schmidt, "Multilevel fast multipole accelerated inverse equivalent current method employing Rao–Wilton–Glisson Discretization of Electric and Magnetic Surface Currents," *IEEE Trans. Antennas Propagat.*, vol. 57, no. 4, pp. 1178–1185, 2009, doi: 10.1109/TAP.2009.2015828.

[22] A. F. Yegulalp, "Fast backprojection algorithm for synthetic aperture radar," in *Proceedings of the IEEE Radar Conference. Radar into the Next Millennium*, Waltham, MA, USA, 1999, pp. 60–65.

[23] Z. Wang, Q. Guo, X. Tian, T. Chang, and H.-L. Cui, "Near-field 3-D millimeter-wave imaging using MIMO RMA with range compensation," *IEEE Trans. Microwave Theory Techn.*, vol. 67, no. 3, pp. 1157–1166, 2019, doi: 10.1109/TMTT.2018.2884409.

[24] M. M. Saurer, B. Hofmann, and T. F. Eibert, "A fully polarimetric multilevel fast spectral domain algorithm for 3-D imaging with irregular sample locations," *IEEE Trans. Microwave Theory Techn.*, vol. 70, no. 9, pp. 4231–4242, 2022, doi: 10.1109/TMTT.2022.3187984.

5. Table of Figures